

PAPER

Asymmetric PSt-EA/Ni-Silicate hollow microsphere with a hierarchical porous shell†

Cite this: *J. Mater. Chem. B*, 2013, **1**, 1414

Yufeng Zhou,^a Wanquan Jiang,^{*a} Shouhu Xuan,^b Xinglong Gong,^{*b} Fang Ye,^a Sheng Wang^a and Qunling Fang^{*c}

Novel asymmetric hollow microspheres with polystyrene-ethylacrylate (PSt-EA) semi-spherical cores and porous hierarchical Ni-Silicate shells have been successfully fabricated by the combination of emulsifier-free polymerization, a modified Stöber method and an *in situ* hydrothermal conversion reaction. During the conversion of the PSt-EA@SiO₂ core/shell microspheres to the asymmetric PSt-EA/Ni-Silicate composite, the spherical PSt-EA was melted within the hollow Ni-Silicate interior to form semi-microspheres. Upon further treating the asymmetric hollow microspheres by 500 °C calcination for 5 h, hierarchical Ni-Silicate hollow spheres were obtained. The BET area of the asymmetric hollow PSt-EA/Ni-Silicate microspheres was 58.9 m² g⁻¹ and the pore diameter was about 10–20 nm. The large porous nature of the products enable them be used as carriers for bio-molecules, and experiments indicated that the maximum adsorption ability of the asymmetric hollow microspheres could reach 8.2 μmol g⁻¹ when the concentration of Cytochrome C was 200 mmol L⁻¹.

Received 8th December 2012

Accepted 7th January 2013

DOI: 10.1039/c2tb00508e

www.rsc.org/MaterialsB

1 Introduction

Nanostructured materials with hollow interiors have attracted extensive attention because of their unique properties, such as high surface area, large pore volume and well-defined pore architecture.^{1,2} Due to their outstanding structural features, these hollow materials could be extended to versatile applications in adsorption, drug delivery, catalysis, chromatography and optical systems.^{3–12} During the past decades, various hollow materials with different morphologies such as nanoparticles,¹³ nanotubes,^{14,15} spindles,¹⁶ microspheres,¹⁷ nanoboxes,¹⁸ etc. have been developed. Most of these functional hollow particles exhibited well-defined porous nanostructures and they could be widely used in biological fields, like medicine sustained-release systems in blood or the body and diagnostic imaging,^{19,20} which is attributed to their multifunctional properties of good water stability and delivery for particular proteins.

The nature of the porous shells is very important for the bio-applications of hollow microspheres.²¹ The surfactant assistant sol-gel method was believed to be the most popular approach

for porous silica nanomaterials because of its easy preparation, green process, and uniform pore distribution.^{22–24} By controlling the carbon chain length of the surfactant, nanoparticles with different pore sizes from 2.4 nm to 3.4 nm were obtained. Large pore size is favorable for immobilization, delivering, and separation of proteins or enzymes due to their large sizes,^{25–28} thus many other methods should be developed to synthesize hollow microspheres with large pores.^{29,30} Yin *et al.* described a surface-protected etching strategy by selectively etching the interior of the silica spheres to yield porous silica hollow spheres.³¹ The pore size can reach as large as 13 nm and meet well with some unique bio-requirements. Recently, hierarchical shells with large pores, which were constructed from tiny nanosheets, have drawn much research interest because of their special nanostructures and functionalities.³² By using SiO₂ as sacrificial templates, hollow metal Silicate spheres with hierarchical porous shells could be effectively achieved.³³ In comparison to the traditional silica and polymer porous hollow spheres, these silicate based hierarchical porous nanomaterials exhibited much higher stability in various chemical environments, high temperatures, and pressures. Moreover, Fe₃O₄ nano-microspheres, CdTe quantum dots, and Pd nanocrystals can be further integrated into this system to give yolk-shell like nanostructures and they exhibited highly promising applications in magnetic separation, imaging, catalysis, and adsorption.^{7,34,35}

Asymmetric nanoarchitectures, often defined as Janus particles, exhibit unique properties by precisely controlling the compositions, hydrophilicity/hydrophobicity, surface charges, and molecular functionalities. Many asymmetric particles, such

^aDepartment of Chemistry, University of Science and Technology of China (USTC), Hefei 230026, PR China. E-mail: jiangwq@ustc.edu.cn; Fax: +86-551-63600419; Tel: +86-551-63607605

^bCAS Key Laboratory of Mechanical Behavior and Design of Materials, Department of Modern Mechanics, USTC, Hefei 230027, PR China. E-mail: gongxl@ustc.edu.cn; Fax: +86-551-63600419; Tel: +86-551-63600419

^cSchool of Medical Engineering, Hefei University of Technology, Hefei 230009, PR China. E-mail: fql.good@hfut.edu.cn; Fax: +86-551-62904405; Tel: +86-551-62904353

† Electronic supplementary information (ESI) available. See DOI: 10.1039/c2tb00508e

as submicron-sized fluorescent spheres, superparamagnetic $\text{Fe}_3\text{O}_4@\text{SiO}_2@\text{polystyrene}$ microspheres, $\text{Fe}_3\text{O}_4\text{-Ag}$ nanocrystals, *etc.*, have been developed for optical probes, spintronic memory devices, and catalysis.^{36,37} Very recently, Gao and Hu³⁸ reported a novel method for making magnetic composite nanoparticles with asymmetric nanostructures, which can be innovatively applied in cancer therapy based on magnetically controlled mechanical forces. However, most Janus particles are solid and few works have been reported on hollow ones. In consideration of the superior characteristics of porous materials, the development of asymmetric hollow particles with hierarchical porous shells is necessary due to their practical applications. Moreover, approaches that can combine the multi-functionalities, uniform size, controllable components, and defined nanostructures together would be also favorable.

In this work, novel asymmetric hollow microspheres (AHMs) with semi-spherical PSt-EA cores and hierarchical porous Ni-Silicate shells were acquired by using an *in situ* template scari-fying-melting method. PSt-EA@ SiO_2 core/shell microspheres, whose size and the shell thickness were tunable, could be employed as the precursor to be converted into AHMs. The resulting composite possesses all the desirable properties, such as hollow interior, porous shell, semi-spherical core with functional surface, high stability, *etc.* The formation mechanism was discussed and this is believed to be a simple and versatile synthetic approach to construct other kind of AHMs with unique functionalities. By using Cytochrome C as an example, the AHMs were proven to be a potential candidate for storing and delivering bio-molecules.

2 Experimental section

2.1 Chemicals

Styrene (St), ethyl acrylate (EA), acrylic acid (AA), potassium persulfate (KPs) tetraethyl orthosilicate (TEOS), ammonium chloride (NH_4Cl), ammonium hydroxide ($\text{NH}_3\cdot\text{H}_2\text{O}$, 25–28%), nickel chloride hexahydrate ($\text{NiCl}_2\cdot 6\text{H}_2\text{O}$) and ethanol were of analytical grade and purchased from Sinopharm Chemical Reagent Co. Ltd. Cytochrome C was purchased from Sangon Biotech (Shanghai) Co. Ltd. The monomer styrene was purified by distillation. Deionized water was used for all experiments.

2.2 Synthesis of asymmetric PSt-EA/Ni-Silicate hollow microsphere and hollow Ni-Silicate microspheres

The PSt-EA nanospheres were formed by soap-free emulsion polymerization.³⁹ Typically, 34 mL styrene (St), 2.6 mL ethyl acrylate (EA), 2.3 mL acrylic acid (AA) and 300 mL deionized water were added to a 500 mL three-necked flask with mechanical stirring for 30 min under nitrogen atmosphere. Then 0.15 g potassium persulfate was introduced as initiator. After mixing, the reactor was heated at 70 °C in a water bath. The PSt-EA product was obtained after 7 h reaction and washed with distilled water three times and then dried in a vacuum oven at 50 °C.

A modified Stöber method was employed to synthesize the core/shell PSt-EA@ SiO_2 microspheres. Firstly, 35 mg PSt-EA

nanospheres were dispersed into a mixture of deionized water (10 mL) and ethanol (5 mL) by ultrasonication for 2 h. The solution was transferred to a 250 mL beaker with $\text{NH}_3\cdot\text{H}_2\text{O}$ (3 mL) and deionized water (82 mL) under magnetic stirring. Then, 2 mL solution of TEOS/ethanol (0.6 mL/10 mL) was injected into the solution every 2 h. After the reaction was performed for 10 h, the obtained products were collected by centrifugation, washed with distilled water and ethanol several times and dried in a vacuum oven at 50 °C. Following the same procedure, the PSt-EA@ SiO_2 microspheres with shell thickness 120 nm were prepared by injecting a solution of TEOS/ethanol (1.2 mL/20 mL) and extending the reaction to 20 h.

The asymmetric PSt-EA/Ni-Silicate hollow microspheres were synthesized by a hydrothermal treatment. 40 mg PSt-EA@ SiO_2 core-shell microspheres were dispersed in 20 mL H_2O under sonication for 2 h. Then, NH_4Cl (0.2673 g), $\text{NiCl}_2\cdot 6\text{H}_2\text{O}$ (0.28 g) and $\text{NH}_3\cdot\text{H}_2\text{O}$ (0.5 mL) were added to the former solution. The solution was further transferred to a 30 mL Teflon-lined autoclave, sealed and maintained at 140 °C for 12 h. After the autoclave cooled to room temperature naturally, the final product AHMs were collected by centrifugation, washed with distilled water and ethanol several times, and dried in a vacuum desiccation oven at 50 °C overnight.

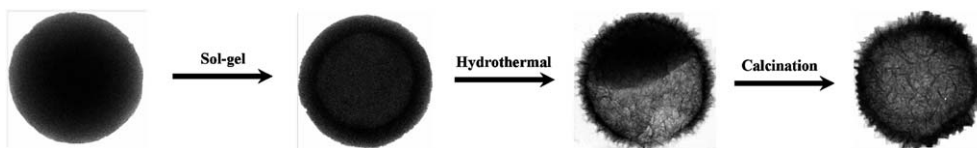
In addition, Ni-Silicate hollow microspheres could be obtained from the calcination of the AHMs at 500 °C for 5 h (Scheme 1).

2.3 Adsorption properties of the AHMs

A series of solutions with standard concentrations ranging from 0.4 to 200 μM were prepared. In each adsorption experiment, 10 mg AHMs were suspended in 20 mL of Cytochrome C solution. The resulting mixture was left for 24 h to reach adsorption equilibrium. The concentration of Cytochrome C was determined spectrophotometrically at a wavelength of 409 nm using UV/vis measurement.

2.4 Measurements and characterization

X-ray powder diffraction (XRD) patterns of the products were obtained with a Japan Rigaku DMax- γA rotating anode X-ray diffractometer equipped with graphite monochromatized Cu $K\alpha$ radiation ($\lambda = 0.154178$ nm). Transmission electron microscopy (TEM) photographs were taken on a JEM-2011 with an accelerating voltage of 200 kV TEM. The field emission scanning electron microscope (FE-SEM, 20 kV) images were taken on a JEOL JSM-6700F SEM. X-ray photoelectron spectra (XPS) were measured on an ESCALAB 250. The UV/vis spectra were recorded by a UV-365 spectrophotometer. Infrared (IR) spectra were recorded in the wave-number range 4000–500 cm^{-1} with a Nicolet Model 759 Fourier transform infrared (FT-IR) spectrometer using a KBr wafer. The nitrogen (N_2) adsorption-desorption isotherms at about 77 K were studied using a Micromeritics, ASAP 2020M system.



Scheme 1 Graphical illustration of the fabrication of hierarchical AHMs and hollow Ni-Silicate microspheres.

3 Results and discussion

Different from the traditional method to synthesize composites with the core eccentrically positioned inside the coating shell, our work developed a facile low temperature melting approach to transform the spherical polymer core to a semi-spherical core within a hollow interior. Interestingly, the hollow nature and the melting of the polymer core took place at the same time, which simplified this method. Firstly, the PSt-EA microspheres were prepared by emulsifier-free polymerization and their surfaces were functionalized with a large amount of carbonyl and hydroxyl groups. Therefore, by using the famous Stöber's method, a uniform SiO₂ shell could be coated onto the PSt-EA to form well dispersed core-shell PSt-EA@SiO₂ microspheres. Then, a hydrothermal treatment was conducted on the above particles and hierarchical PSt-EA/Ni-Silicate AHMs with both hollow interiors and asymmetric nanostructures were obtained. After heating the AHMs powder at 500 °C for 5 h, we obtained the hollow Ni-Silicate microspheres.

The crystalline structures of products obtained at each step were characterized by XRD. Fig. 1a shows the XRD pattern of the PSt-EA microspheres. Similar to the previous report,⁴⁰ two diffraction peaks located at 10° and 18° which can be attributed to the polymeric phase of the materials were observed, indicating the formation of PSt-EA microspheres by the soap-free emulsion polymerization. After coating with the SiO₂ shell, a broad peak at ~24° was found as shown in Fig. 1b. This diffraction peak corresponds to amorphous silica,⁴¹ confirming that the obtained microspheres consisted of amorphous silica and PSt-EA. As soon as the PSt-EA@SiO₂ core-shell microspheres were transformed into AHMs, only sharp

peaks located at 20°, 34°, 39° and 53° were observed (Fig. 1c) and they were indexed to be silicate hydroxide hydrate hexagonal phase (JCPDS no. 43-0664, Ni₃Si₄O₁₀(OH)₂·5H₂O, this substance was defined as Ni-Silicate in this work for simplicity).⁴² Definitely, the broad nature of the diffraction peak indicates the low crystallinity of the final silicate. To further investigate the compositions of the obtained products, the XPS spectra were recorded (Fig. 2). As shown in Fig. 2a, two peaks of C1s and O1s at 285 eV and 520 eV were derived from the PSt-EA microspheres. When the SiO₂ layer was coated on the PSt-EA core, the intensity of the C1s signal decreased sharply while the O1s peak increased markedly. In combination with the presence of the Si2p peak located at 104 eV, it could be concluded that the uniform core-shell structure was successfully achieved. After further hydrothermal treatment of the PSt-EA@SiO₂ core-shell microspheres in the Ni²⁺ based solution, the SiO₂ shell was transformed to nickel silicate, which corresponded well with the XPS spectra for the appearance of Si2p and Ni2p peaks at 104 eV and 855 eV, respectively.

Fig. 3a is the low magnification TEM image of the as-prepared AHMs, which clearly shows that all the products exhibited a spherical morphology. These microspheres were very uniform and the average size was about 600 nm. Interestingly, about half of the microsphere exhibited a gray color within the dark black shell and the other hemi-sphere was brighter, which indicated that these hybrid microspheres presented an asymmetric nanostructure (Fig. 3b). Fig. 3c shows a typical TEM image of the AHMs, in which an arc interface

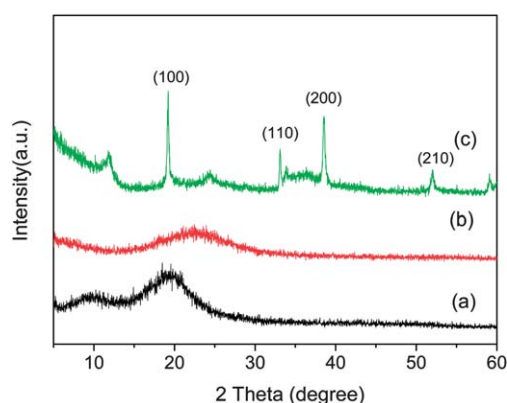


Fig. 1 The XRD patterns of PSt-EA microspheres (a), PSt-EA@SiO₂ core-shell microspheres (b), and AHMs (c).

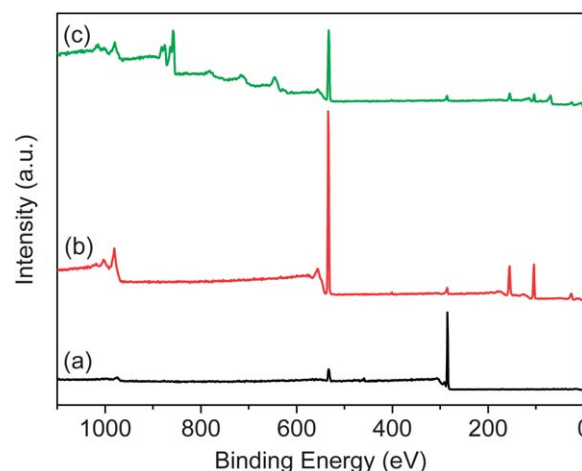


Fig. 2 The XPS spectra of PSt-EA microspheres (a), PSt-EA@SiO₂ core-shell microspheres (b), and AHMs (c).

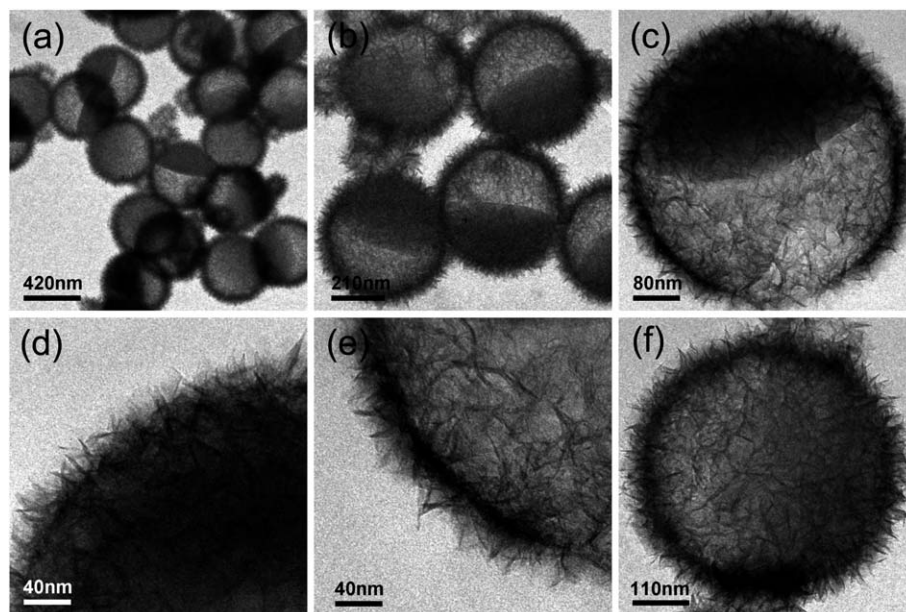


Fig. 3 The TEM images of the AHM microspheres with different magnifications (a–f).

between the two hemi-spheres was clearly observed. The gray hemi-sphere was formed by melting the PSt-EA microsphere within a spherical space thus the other part must be a hollow interior. A TEM image with higher magnification (Fig. 3d) clearly reveals that the hemi-spherical PSt-EA particle connected well with the outer shell. Although no clear interface could be found due to the similarity of the TEM image contrast, the hemi-spherical PSt-EA core and the silicate shell were definitely distinguished because of their different nanostructures. Shown in Fig. 3e is the TEM image of the silicate shell located in the hollow part, which indicates that the silicate shell was composed of a large number of nanosheets with thicknesses of several nanometres. These nanosheets were randomly packed thus the hierarchical porous nanostructure was formed due to the inter-particle attachment. Importantly, the PSt-EA core was well confined within the hierarchical porous silicate shell without any diffusion. These results also proved that the PSt-EA microsphere was well cross-linked and they could be only softened during the hydrothermal treatment. Moreover, when the cross-section face of the semi-polymer core was parallel to the TEM beam, the image exhibited a clear semi-hollow nature. However, if the cross-section face of the polymer core was perpendicular to the TEM beam, the particle would show a core-shell like image. Fig. 3f shows a particle where the cross-section face was moved from the parallel position, thus a gibbous-shaped core was found.

To analyze the synthesis mechanism, both SEM and TEM were used to track the product in each step. Fig. 4a represents a typical SEM image of as-prepared PSt-EA microspheres, indicating that the sample has spherical structure with uniform diameter of about 310 nm. The PSt-EA microspheres with fine dispersity and narrow size distribution are also clearly observed from the TEM image (Fig. 4b), which agreed well with the SEM analysis. The modified Stöber method was

used for coating SiO₂ shells on PSt-EA microspheres. As shown in Fig. 4c, the PSt-EA@SiO₂ composite microspheres were about 450 nm and they could pack to form a hexagonal structure on the copper plate, which clearly indicated the size

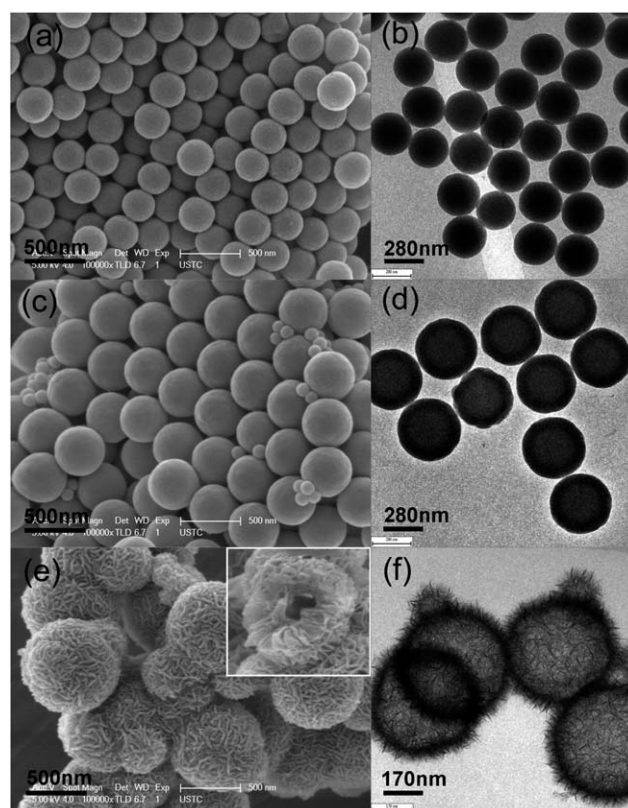


Fig. 4 The SEM and TEM images of the PSt-EA microspheres (a and b), PSt-EA@SiO₂ microspheres (c and d), AHMs (e), and hollow Ni-Silicate microspheres (f).

distribution of the product was very uniform. Unfortunately, some SiO₂ nanospheres with diameter of 80 nm were also found in the SEM image, which must be formed during the sol-gel progress due to the self-nucleation of the TEOS. From the TEM image (Fig. 4d), we could find the as-prepared microspheres exhibited a clear core/shell nanostructure and the shell thickness was about 80 nm. In this work, the shell thickness can be controlled by simply varying the concentration of the TEOS precursor. Shown in Fig. S1† are the PSt-EA@SiO₂ samples with 80 nm and 120 nm shell thicknesses, and the core/shell particles were also well dispersed without any shell coalescence.

A hydrothermal reaction was conducted to convert the PSt-EA@SiO₂ core-shell microspheres to PSt-EA/Ni-Silicate asymmetric hollow microspheres. The SEM image (Fig. 4e) shows that the average size of the AHMs was about 600 nm, in good agreement with the TEM analysis. The surface of the microspheres is composed of many sheet-like nanocrystals, thus the product exhibited a flower-like hierarchical nanostructure. The inset of Fig. 4e is the SEM image of a broken particle, which clearly indicates the hollow nature of the AHMs. Here, if the shell thickness of the PSt-EA@SiO₂ increased, both the inner diameter of the AHMs and the final silicate shell thickness increased (Fig. S2†). With further calcination of the hierarchical PSt-EA/Ni-Silicate microspheres at 500 °C for 5 h, the PSt-EA cores were decomposed at high temperature and only Ni-Silicate hollow microspheres could be achieved. As shown in Fig. 3f, the hierarchical sheet-like nanostructure of the Ni-Silicate shell was well retained and the hollow interior was also conserved.

Fig. 5a shows the FT-IR spectroscopy of the PSt-EA microspheres, in which the bands at 1630 and 1710 cm⁻¹ were attributed to the stretching vibrations of the vinyl and carbonyl groups, respectively. A strong characteristic absorption band at 1100 cm⁻¹ was found in Fig. 5b and these peaks were attributed to the Si-O-Si bond, which indicated the SiO₂ layer was coated on the PSt-EA to form PSt-EA@SiO₂ microspheres. After the further hydrothermal process, a band located at 1024 cm⁻¹ was present in Fig. 5c. Clearly, it was derived from the Si-O vibration of the hierarchical Ni-Silicate shell. Fig. 6 illustrates the result of

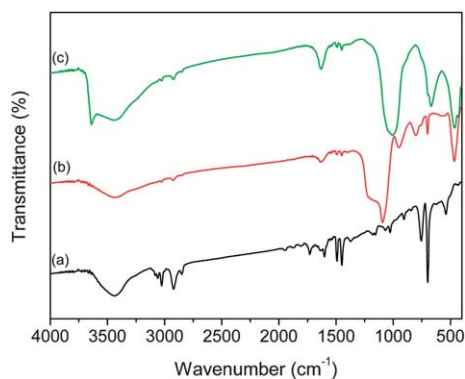


Fig. 5 The FT-IR spectra of PSt-EA microspheres (a), PSt-EA@SiO₂ microspheres (b), and AHMs (c).

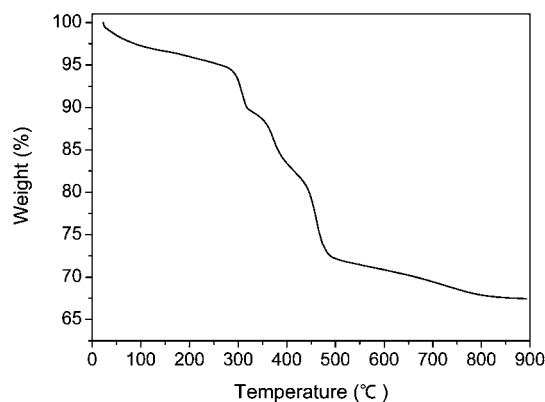


Fig. 6 TG of the as-prepared AHM microspheres.

the thermogravimetric analysis of the PSt-EA/Ni-Silicate AHMs. The first weight loss from 100 to 300 °C resulted from the evaporation of adsorbed water. The weight loss at higher temperature (300–500 °C) could be attributed to the decomposition of PSt-EA cores, where the weight reduced to 71%. The weight loss (300–500 °C) includes several weight losses due to the different degrees of polymerization of PSt-EA. When the temperature was increased to 900 °C, the slight weight loss could be attributed to the residual polymer and crystallized water.

In this work, the hydrothermal treatment played a critical role in the preparation of the AHMs. This reaction was conducted within an alkaline medium in the presence of Ni²⁺. Under high temperature and pressure, the surface SiO₂ of the PSt-EA@SiO₂ microspheres was firstly dissolved to form silicate anions which would quickly react with the Ni²⁺ to give nickel silicate nucleation. These nanograins preferred to deposit on the periphery of the PSt-EA@SiO₂ microspheres and continuously grow to form the nanosheets. Thereafter, the nanosheets randomly packed to form hierarchical porous shells and thus the inner diameter would be equal to the diameter of the PSt-EA@SiO₂ microsphere. As soon as the SiO₂ coating was consumed, the PSt-EA microspheres would attach to the inner interface of the Ni-Silicate shell. At high temperature, the PSt-EA microspheres were softened and transformed into semi-spherical particles within the spherical capsules due to gravity. Because of the cross-linking nature of the PSt-EA and the hydrophobic effect, these PSt-EA microspheres remained within the hollow interior without outflow. Finally, the asymmetric hollow microspheres with porous shells were successfully prepared by using the *in situ* template scarifying-melting method.

The obtained PSt-EA/Ni-Silicate microspheres presented semi-hollow nature and the Ni-Silicate shell was randomly packed with a large amount of nanosheets, thus it was believed that the product possessed excellent surface area. The nitrogen adsorption-desorption isotherm and BJH pore plot of the AHMs were recorded to evaluate the porous properties of the sample (Fig. 7). Obviously, the nitrogen adsorption-desorption isotherm shows a typical type-IV curve, indicating the presence of interparticle and nonordered mesoporosity in the

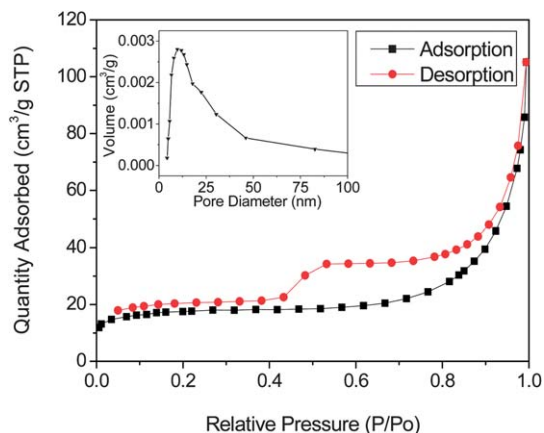


Fig. 7 Nitrogen adsorption–desorption isotherm and BJH pore plot (inset) of the as-prepared AHMs.

sample. According to the BJH pore distribution curve (inset in Fig. 7), the major pore size is found to be 12 nm. The BET surface area of the asymmetric hollow microspheres is $58.9 \text{ m}^2 \text{ g}^{-1}$, which must correspond to the mesopores from the hierarchical shell and the hollow interior of the composite particle.

Due to the large pore size, hollow interior, and the large BET surface areas, the as-prepared PSt-EA/Ni-Silicate microspheres could have potential applications in adsorption for protein macromolecules. Here, Cytochrome C was chosen as a typical bio-molecule for study and the adsorption plot of Cytochrome C into the semi-hollow PSt-EA/Ni-Silicate microspheres is shown in Fig. 8. After the equilibration for 24 h, it was found that the AHMs were effective for the adsorption. With increasing Cytochrome C concentration, the adsorption capability firstly increased sharply. When the Cytochrome C concentration was greater than 100 mmol L^{-1} , the adsorption tended level off and the maximum adsorption could reach $8.2 \text{ } \mu\text{mol g}^{-1}$ when the concentration was 200 mmol L^{-1} . The high surface area in the void space of the porous shell and hollow interior make this kind of particle an ideal candidate for bio-separation.

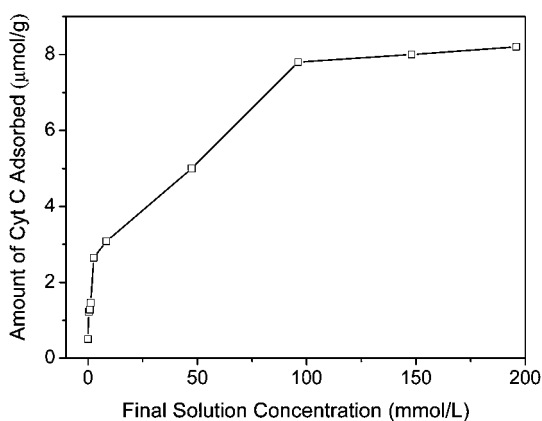


Fig. 8 Adsorption of Cytochrome C on PSt-EA/Ni-Silicate AHMs at different solution concentrations.

4 Conclusion

In summary, we demonstrated a facile preparation of asymmetric hollow microspheres with PSt-EA semi-spherical cores and Ni-Silicate hierarchical porous shells. AHMs with tunable size could be obtained by varying the thicknesses of the SiO_2 coating on the PSt-EA microspheres. By investigating the product under each step, the *in situ* template scarifying–melting mechanism was studied. Due to the hollow interior and porous shell, the asymmetric hollow PSt-EA/Ni-Silicate microspheres exhibited high BET surface areas. Toward the bio-adsorption application, we found the maximum adsorption capability of the AHMs for Cytochrome C could reach to $8.2 \text{ } \mu\text{mol g}^{-1}$ at a Cytochrome C concentration of 200 mmol L^{-1} . These asymmetric nanostructures and their derivatives would be very interesting in the future for assembling other new types of multi-functional platforms for catalysis, sensing, and enzyme immobilization, which have attracted much attention.

Acknowledgements

Financial support from the National Natural Science Foundation of China (Grant no.21205026, 11072234, 11125210) and the National Basic Research Program of China (973 Program, Grant no. 2012CB937500) is gratefully acknowledged.

References

- 1 M. Sanlés-Sobrido, M. Pérez-Lorenzo, B. Rodríguez-González, V. Salgueiriño and M. A. Correa-Duarte, *Angew. Chem., Int. Ed.*, 2012, **51**, 3877.
- 2 S. A. Dergunov and E. Pinkhassik, *J. Am. Chem. Soc.*, 2011, **133**, 19656.
- 3 H. Q. Wang, M. Miyauchi, Y. Ishikawa, A. Pyatenko, N. Koshizaki, Y. Li, L. Li, X. Y. Li, Y. Bando and D. Golberg, *J. Am. Chem. Soc.*, 2011, **133**, 19102.
- 4 T. X. Nguyen and S. K. Bhatia, *Carbon*, 2012, **50**, 3045.
- 5 W. M. Yang, L. K. Liu, W. Zhou, W. Z. Xu, Z. P. Zhou and W. H. Huang, *Appl. Surf. Sci.*, 2012, **258**, 6583.
- 6 C. J. Ke, Y. J. Lin, Y. C. Hu, W. L. Chiang, K. J. Chen, W. C. Yang, H. L. Liu, C. C. Fu and H. W. Sung, *Biomaterials*, 2012, **33**, 5156.
- 7 M. Changez, N. G. Kang and J. S. Lee, *Small*, 2012, **8**, 1173.
- 8 C. Kim, S. Kim, W. K. Oh, M. Choi and J. Jang, *Chem.–Eur. J.*, 2012, **18**, 4902.
- 9 X. L. Fang, Z. H. Liu, M. F. Hsieh, M. Chen, P. X. Liu, C. Chen and N. F. Zheng, *ACS Nano*, 2012, **6**, 4434.
- 10 F. Bai, Z. C. Sun, M. S. Wu, R. E. Haddad, X. Y. Xiao and H. Y. Fan, *Nano Lett.*, 2011, **11**, 3759.
- 11 D. Ge and H. K. Lee, *J. Chromatogr., A*, 2012, **1229**, 1.
- 12 C. Rajapakse, F. Wang, T. C. Y. Tang, P. J. Reece, S. G. Leon-Saval and A. Argyros, *Opt. Express*, 2012, **20**, 11232.
- 13 F. Q. Tang, L. L. Li and D. Chen, *Adv. Mater.*, 2012, **24**, 1504.
- 14 L. X. Ding, A. L. Wang, G. R. Li, Z. Q. Liu, W. X. Zhao, C. Y. Su and Y. X. Tong, *J. Am. Chem. Soc.*, 2012, **134**, 5730.
- 15 M. Olek, J. Ostrander, S. Jurga, H. Möhwald, N. Kotov, K. Kempa and M. Giersig, *Nano Lett.*, 2004, **4**, 1889.

- 16 W. Q. Cai, J. G. Yu and M. Jaroniec, *J. Mater. Chem.*, 2010, **20**, 4587.
- 17 Y. H. Deng, Y. Cai, Z. K. Sun, J. Liu, C. Liu, J. Wei, W. Li, C. Liu, Y. Wang and D. Y. Zhao, *J. Am. Chem. Soc.*, 2010, **132**, 8466.
- 18 Z. Y. Wang, D. Y. Luan, F. Y. C. Boey and X. W. Lou, *J. Am. Chem. Soc.*, 2011, **133**, 4738.
- 19 N. Singh, A. Karambelkar, L. Gu, K. Lin, J. S. Miller, C. S. Chen, M. J. Sailor and S. N. Bhatia, *J. Am. Chem. Soc.*, 2011, **133**, 19582.
- 20 C. M. Hessel, M. R. Rasch, J. L. Hueso, B. W. Goodfellow, V. A. Akhavan, P. Puvanakrishnan, J. W. Tunnel and B. A. Korgel, *Small*, 2010, **6**, 2026.
- 21 J. P. Ge, Q. Zhang, T. R. Zhang and Y. D. Yin, *Angew. Chem., Int. Ed.*, 2008, **47**, 8924.
- 22 Y. Q. Wang, C. J. Tang, Q. Deng, C. H. Liang, D. H. L. Ng, F. L. Kwong, H. Q. Wang, W. P. Cai, L. D. Zhang and G. Z. Wang, *Langmuir*, 2010, **26**, 14830.
- 23 W. R. Zhao, M. D. Lang, Y. S. Li, L. Li and J. L. Shi, *J. Mater. Chem.*, 2009, **19**, 2778.
- 24 X. J. Wu and D. S. Xu, *J. Am. Chem. Soc.*, 2009, **131**, 2774.
- 25 Y. Pan, M. J. C. Long, X. M. Li, J. F. Shi, L. Hedstrom and B. Xu, *Chem. Sci.*, 2011, **2**, 945.
- 26 L. Zhang, S. Z. Qiao, Y. G. Jin, H. G. Yang, S. Budihartono, F. Stahr, Z. F. Yan, X. L. Wang, Z. P. Hao and G. Q. Lu, *Adv. Funct. Mater.*, 2008, **18**, 3203.
- 27 Y. H. Deng, C. H. Deng, D. W. Qi, C. Liu, J. Liu, X. M. Zhang and D. Y. Zhao, *Adv. Mater.*, 2009, **21**, 1377.
- 28 Y. Q. Wang, G. Z. Wang, H. Q. Wang, W. P. Cai, C. H. Liang and L. D. Zhang, *Nanotechnology*, 2009, **20**, 155604.
- 29 D. Chen, L. L. Li, F. Q. Tang and S. Qi, *Adv. Mater.*, 2009, **21**, 3804.
- 30 Y. Chen, H. R. Chen, L. M. Guo, Q. J. He, F. Chen, J. Zhou, J. W. Feng and J. L. Shi, *ACS Nano*, 2010, **4**, 529.
- 31 Q. Zhang, T. R. Zhang, J. P. Ge and Y. D. Yin, *Nano Lett.*, 2008, **8**, 2867.
- 32 Y. Q. Wang, G. Z. Wang, H. Q. Wang, C. H. Liang, W. P. Cai and L. D. Zhang, *Chem.–Eur. J.*, 2010, **16**, 3497.
- 33 J. Zheng, B. H. Wu, Z. Y. Jiang, Q. Kuang, X. L. Fang, Z. X. Xie, R. B. Huang and L. S. Zheng, *Chem.–Asian J.*, 2010, **5**, 1439.
- 34 M. Kim, J. C. Park, A. Kim, K. H. Park and H. Song, *Langmuir*, 2012, **28**, 6441.
- 35 P. Yang, M. Ando and N. Murase, *New J. Chem.*, 2009, **33**, 561.
- 36 C. L. Wang, J. T. Yan, X. J. Cui and H. Y. Wang, *J. Colloid Interface Sci.*, 2011, **354**, 94.
- 37 Y. Pan, J. H. Gao, B. Zhang, X. X. Zhang and B. Xu, *Langmuir*, 2010, **26**, 4184.
- 38 S. H. Hu and X. H. Gao, *J. Am. Chem. Soc.*, 2010, **132**, 7234.
- 39 Y. Wi, K. Lee, B. H. Lee and S. Choe, *Polymer*, 2008, **49**, 5626.
- 40 F. M. Uhl and C. A. Wilkie, *Polym. Degrad. Stab.*, 2002, **76**, 111.
- 41 X. P. Zhang, W. Q. Jiang, Y. F. Zhou, S. H. Xuan, C. Peng, L. H. Zong and X. L. Gong, *Nanotechnology*, 2011, **22**, 375701.
- 42 Q. L. Fang, S. H. Xuan, W. Q. Jiang and X. L. Gong, *Adv. Funct. Mater.*, 2011, **21**, 1902.